Analytical Solution for Whirling Speeds and Mode Shapes of a Distributed-Mass Shaft With Arbitrary Rigid Disks

Jong-Shyong Wu[1]
e-mail: jswu@mail.ncku.edu.tw

Foung-Tang Lin

Huei-Jou Shaw

Department of Systems and Naval
Mechatronic Engineering,
National Cheng-Kung University,
Tainan 701, Taiwan

The purpose of this paper is to present an approach for replacing the effects of each rigid disk mounted on the spin shaft by a lumped mass together with a frequency-dependent equivalent mass moment of inertia so that the whirling motion of a rotating shaft-disk system is similar to the transverse free vibration of a stationary beam and the technique for the free vibration analysis of a stationary beam with multiple concentrated elements can be used to determine the forward and backward whirling speeds, along with mode shapes of a distributed-mass shaft carrying arbitrary rigid disks. Numerical results reveal that the characteristics of whirling motions are significantly dependent on the slopes of the associated natural mode shapes at the positions where the rigid disks are located. Furthermore, the results obtained from the presented analytical method and those obtained from existing literature or the finite element method (FEM) are in good agreement. [DOI: 10.1115/1.4024670]

1 Introduction

The critical speeds of flexible rotors are important information for many engineers; thus, there is great amount of literature concerning this subject. The existing literature reveals that the dynamic problems of rotor-bearing systems are solved by the step-by-step integration process [1], transfer matrix method (TMM) [2], analytical method [3–5], assumed mode method [6], hybrid method [7], frequency-dependent TMM [8] or the finite element method (FEM) [9,10]. Besides, Yamamoto and Ishida [11] have introduced the applications of the analytical methods, the TMM and FEM, to the linear and nonlinear dynamics of multi-disk rotor-bearing systems.

From the foregoing literature reviews, one sees that all existing techniques for the analysis of whirling motions are the approximate approaches except for the analytical method presented by Eshleman and Eubanks [4] and that introduced by Yamamoto and Ishida [11]. In theory, the solution of Eshleman and Eubanks [4] is an *exact* one, however, it is only for the whirling speeds of a rotating shaft carrying "one" disk and the corresponding "whirling mode shapes" are not considered. Thus, the purpose of this paper is to extend and modify the aforementioned technique, so that the lowest five (or higher) forward and backward whirling speeds and the associated mode shapes for a shaft carrying any number of disks with various boundary conditions can be easily obtained. To this end, the transverse displacement of each shaft cross-section is represented by a complex number and then the equation of motion, the continuity equations for the deformations, the equilibrium equations for the forces (and moments), and the associated boundary conditions are derived in terms of the complex numbers in which the effects of each rigid disk mounted on the spin shaft are replaced by a lumped mass and a *frequency-dependent* equivalent mass moment of inertia. Finally, the method for obtaining the natural frequencies and mode shapes of a *stationary* beam carrying multiple concentrated elements [12–14] is used to determine the forward and backward whirling speeds and mode shapes of a *spinning* shaft mounted by arbitrary rigid disks. In addition to a comparison with the existing literature, most of the results obtained from the presented method are also compared with those obtained from the FEM by using the technique shown in the Appendix with the property matrices of each shaft element and each rigid disk given by Nelson and McVaugh [9] and Przemieniecki [15].

A structural system may be considered as the "continuous" system or "discrete" system and the solution obtained from the former is called the "closed-form" or "exact" solution, while that from the latter is called the "approximate" solution [16]. Thus, the results obtained from the proposed method are the "exact" solutions and may be the "benchmark" for evaluating the accuracy of the other "approximate" solutions such as those obtained from the FEM.

2 Formulations for the Problem

2.1 Equation of Motion and Displacement Function for a Shaft Segment. Figure 1 shows a multistep shaft with its two ends supported by ball bearings. It consists of n uniform shaft segments (denoted by (1), (2), …, $(i-1)$, (i), $(i+1)$, …, (n)) separated by $n-1$ nodes (denoted by 1, 2, …, $i-1$, i, $i+1$, …, $n-1$) and carrying a rigid disk $m_{d,i}$ (with an *equivalent* mass moment of inertia $J_{\text{eq},i}$) at each node i, for $i=1$ to $n-1$. Figure 2 shows the coordinate systems for the rotating shaft with a spin speed Ω about its longitudinal (a-) axis and a whirling speed $\tilde{\omega}$ about the centerline of the bearings (x-axis), where xyz, $\tilde{x}\tilde{y}\tilde{z}$, and abc are the non-rotating (space-fixed), rotating (shaft-fixed), and cross-sectional coordinate systems, respectively. The relative positions between the xyz and $\tilde{x}\tilde{y}\tilde{z}$ coordinate systems are determined by the angle $\theta_x = \tilde{\omega}t$ and the position of the abc coordinate system is defined by θ_x, θ_y, θ_z, and the axial coordinate x. Besides, u_y and u_z are the vertical and horizontal transverse displacements of the cross-sectional centroid of the shaft (or the center of gravity of the disk) in the y- and z-directions, while θ_y and θ_z are the rotational angles of the shaft (or disk) cross-section (located at x) about the y- and z-axes, respectively.

For the ith shaft segment (see Fig. 1), its equations of motion during whirling are given by

$$E_i I_i \frac{\partial^4 u_{y,i}(x,t)}{\partial x^4} + \rho_i A_i \frac{\partial^2 u_{y,i}(x,t)}{\partial t^2} = 0 \quad (\text{for } x_{i-1} \le x \le x_i) \tag{1a}$$

$$E_i I_i \frac{\partial^4 u_{z,i}(x,t)}{\partial x^4} + \rho_i A_i \frac{\partial^2 u_{z,i}(x,t)}{\partial t^2} = 0 \quad (\text{for } x_{i-1} \le x \le x_i) \tag{1b}$$

where ρ_i, E_i, and A_i are the mass density, Young's modulus, and the cross-sectional area of the ith shaft segment, respectively, I_i is the *diametric* moment of inertia of area A_i, while $u_{y,i}(x, t)$ and $u_{z,i}(x, t)$ are the vertical and horizontal displacements for the centroid of the cross-section of the ith shaft segment at the axial coordinate x and time t (see Fig. 2), respectively.

Let

$$u_i(x,t) = u_{y,i}(x,t) + j u_{z,i}(x,t) \tag{2}$$

with $j = \sqrt{-1}$, then, Eqs. (1*a*) and (1*b*) become

[1]Corresponding author.

Manuscript received November 16, 2011; final manuscript received May 12, 2013; accepted manuscript posted May 29, 2013; published online September 19, 2013. Assoc. Editor: Alexander F. Vakakis.

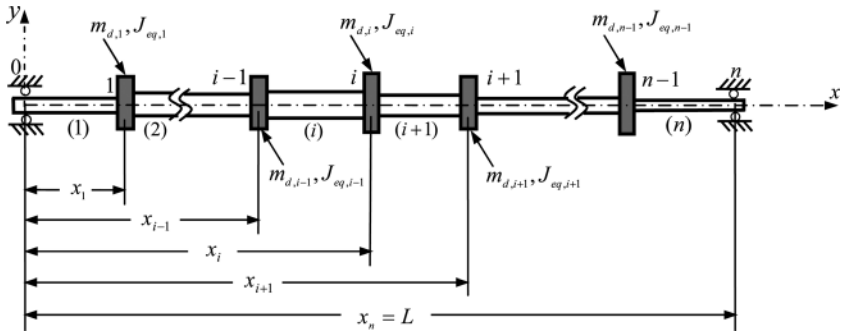

Fig. 1 A multistep bearing-support shaft composed of *n* uniform shaft segments (denoted by (1), (2), . . ., (*i* − 1), (*i*), (*i* + 1), . . ., (*n*)) separated by *n* − 1 nodes (denoted by 1, 2, . . ., *i* − 1, *i*, *i* + 1, . . ., *n* − 1) and carrying a rigid disk $m_{d,i}$ (with equivalent mass moments of inertia $J_{eq,i}$) at each node *i*, for *i* = 1 to *n* − 1

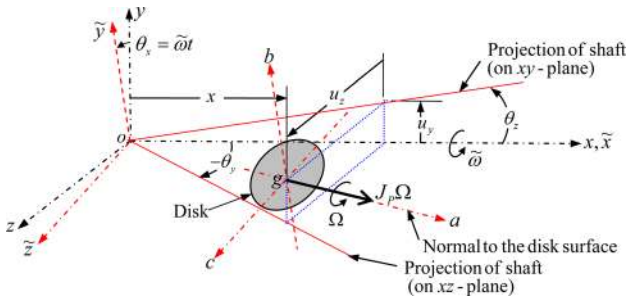

Fig. 2 The coordinate systems for a rotating shaft with spin speed Ω about the *a*-axis and whirling speed $\tilde{\omega}$ about the *x*-axis with *xyz*, $\tilde{x}\tilde{y}\tilde{z}$, and *abc* denoting the space-fixed, shaft-fixed and cross-sectional coordinate systems, respectively

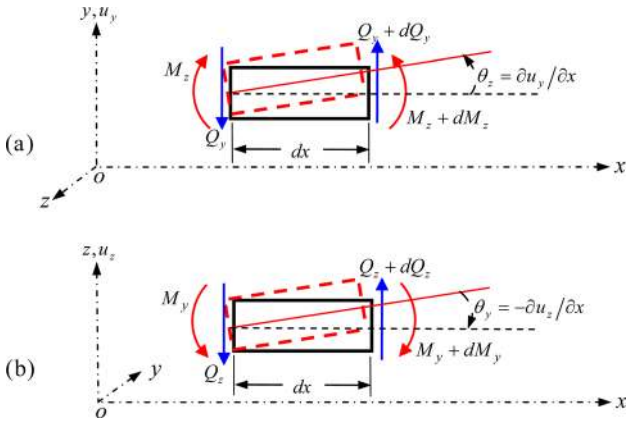

Fig. 3 Free-body diagrams for the "shaft segment" *dx* on (*a*) the *xy*-plane, and (*b*) the *xz*-plane

$$E_i I_i \frac{\partial^4 u_i(x,t)}{\partial x^4} + \rho_i A_i \frac{\partial^2 u_i(x,t)}{\partial t^2} = 0 \quad (\text{for } x_{i-1} \le x \le x_i) \tag{3}$$

For the free vibrations, one has

$$u_i(x,t) = U_i(x) e^{\pm j\tilde{\omega}t} \tag{4}$$

where $U_i(x)$ is the amplitude function of the *i*th shaft segment and $\tilde{\omega}$ is the whirling speed of the entire shaft-disk system about the centerline of the bearings (the fixed *x*-axis). Furthermore, the upper sign (+) and lower sign (−) are for the forward and backward whirls, respectively.

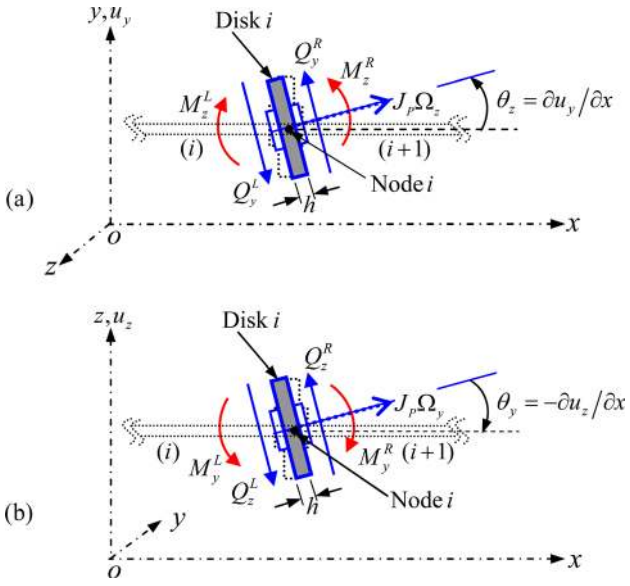

Fig. 4 Free-body diagrams for the "rigid disk" *i* located at node *i* (with axial coordinate $x = x_i$) joining shaft segments (*i*) at left side and (*i* + 1) at the right side on (*a*) the *xy*-plane, and (*b*) the *xz*-plane. The superscripts *L* and *R* refer to the left and right sides of disk *i*, respectively.

Substituting Eq. (4) into Eq. (3) leads to

$$U_i''''(x) - \beta_i^4 U_i(x) = 0 \quad (\text{for } x_{i-1} \le x \le x_i) \tag{5}$$

with

$$\beta_i^4 = \tilde{\omega}^2 \rho_i A_i / (E_i I_i) \tag{6}$$

where the prime (′) denotes differentiation with respect to the axial coordinate *x*.

The solution of Eq. (5) takes the form

$$U_i(x) = A_i \sinh \beta_i x + B_i \cosh \beta_i x + C_i \sin \beta_i x + D_i \cos \beta_i x \quad (\text{for } x_{i-1} \le x \le x_i) \tag{7}$$

2.2 Equilibrium Equations for Forces and Moments at Arbitrary Intermediate Node *i*. The entire shaft-disk system is composed of "shaft segments" and "rigid disks," as shown in Fig. 1. The free-body diagrams for a typical "shaft segment" *dx* on the *xy*- and *xz*-planes are shown in Figs. 3(*a*) and 3(*b*), respectively, while those for a typical "rigid disk" *i* located at node *i* (with $x = x_i$) joining shaft segments (*i*) at the left side and (*i* + 1) at the right side on the *xy*- and *xz*-planes are shown in Figs. 4(*a*) and 4(*b*), respectively.

From Figs. 3(*a*) and 3(*b*), one obtains

$$\theta_y = -\frac{\partial u_z}{\partial x} \tag{8a}$$

$$\theta_z = \frac{\partial u_y}{\partial x} \tag{8b}$$

$$M_y = -EI_y \frac{\partial^2 u_z}{\partial x^2} \tag{9a}$$

$$M_z = EI_z \frac{\partial^2 u_y}{\partial x^2} \tag{9b}$$

$$Q_y = -\frac{\partial M_z}{\partial x} = -EI_z \frac{\partial^3 u_y}{\partial x^3} \tag{10a}$$

$$Q_z = \frac{\partial M_y}{\partial x} = -EI_y \frac{\partial^3 u_z}{\partial x^3} \tag{10b}$$

If the displacements are small and the center of gravity (c.g.) of each disk is coincident with the centroid of the cross-section of the shaft segment then for the translational motions, from Figs. 4(*a*) and 4(*b*), one has

$$Q_y^R - Q_y^L = m_{d,i} \frac{\partial^2 u_y(x_i,t)}{\partial t^2} \tag{11a}$$

$$Q_z^R - Q_z^L = m_{d,i} \frac{\partial^2 u_z(x_i,t)}{\partial t^2} \tag{11b}$$

where $m_{d,i}$ is the mass of the rigid disk i located at node i (with $x = x_i$), while Q_y and Q_z are shearing forces on the rigid disk i in the y- and z-directions, respectively, with the superscripts R and L denoting the right side and the left side of the disk i (or node i). Similarly, for the rotational motions, from Figs. 4(*a*) and 4(*b*), one has

$$M_z^R - M_z^L = J_{D,i} \frac{\partial^2 \theta_z(x_i,t)}{\partial t^2} + J_{P,i} \frac{\partial \Omega_z}{\partial t} \tag{12a}$$

$$M_y^R - M_y^L = J_{D,i} \frac{\partial^2 \theta_y(x_i,t)}{\partial t^2} + J_{P,i} \frac{\partial \Omega_y}{\partial t} \tag{12b}$$

where $J_{D,i}$ and $J_{P,i}$ are the diametric and polar mass moments of inertia of the rigid disk i, respectively, and $\partial(J_{P,i}\Omega_k)/\partial t = J_{P,i}(\partial\Omega_k/\partial t)$ is the time rate of change of angular momentum for the disk i in the k-direction (with $k = y$ or z) and Ω_y and Ω_z are the components of the spin speed Ω of the shaft and disk in the y- and z-directions, respectively, given by (see Figs. 2 and 4)

$$\Omega_y = \Omega \sin\theta_z \approx \Omega\theta_z \tag{13a}$$

$$\Omega_z = \Omega \sin(-\theta_y) \approx -\Omega\theta_y \tag{13b}$$

Substituting Eqs. (13*a*) and (13*b*) into Eqs. (12*a*) and (12*b*), respectively, one obtains

$$M_z^R - M_z^L = J_{D,i} \frac{\partial^2 \theta_z(x_i,t)}{\partial t^2} - J_{P,i}\Omega \frac{\partial \theta_y(x_i,t)}{\partial t} \tag{14a}$$

$$M_y^R - M_y^L = J_{D,i} \frac{\partial^2 \theta_y(x_i,t)}{\partial t^2} + J_{P,i}\Omega \frac{\partial \theta_z(x_i,t)}{\partial t} \tag{14b}$$

Similarly, substituting Eqs. (10*a*) and (10*b*) into Eqs. (11*a*) and (11*b*), respectively, yields

$$-EI_z \frac{\partial^3 u_y^R(x_i,t)}{\partial x^3} + EI_z \frac{\partial^3 u_y^L(x_i,t)}{\partial x^3} - m_{d,i} \frac{\partial^2 u_y(x_i,t)}{\partial t^2} = 0 \tag{15a}$$

$$-EI_y \frac{\partial^3 u_z^R(x_i,t)}{\partial x^3} + EI_y \frac{\partial^3 u_z^L(x_i,t)}{\partial x^3} - m_{d,i} \frac{\partial^2 u_z(x_i,t)}{\partial t^2} = 0 \tag{15b}$$

Introducing Eq. (2) into Eqs. (15*a*) and (15*b*) leads to

$$-EI \frac{\partial^3 u^R(x_i,t)}{\partial x^3} + EI \frac{\partial^3 u^L(x_i,t)}{\partial x^3} - m_{d,i} \frac{\partial^2 u(x_i,t)}{\partial t^2} = 0 \tag{16}$$

or

$$E_i I_i u_i'''(x_i,t) = E_{i+1} I_{i+1} u_{i+1}'''(x_i,t) + m_{d,i} \ddot{u}_i(x_i,t) \tag{17}$$

which is the equilibrium equation for the shearing forces on disk i (located at node i), where the overhead dot $(\cdot)$ denotes differentiation with respect to time t, while $\partial^3 u^L(x_i,t)/\partial x^3 = u_i'''(x_i,t)$, $\partial^3 u^R(x_i,t)/\partial x^3 = u_{i+1}'''(x_i,t)$, $\partial^2 u^L(x_i,t)/\partial t^2 \equiv \partial^2 u^R(x_i,t)/\partial t^2 = \ddot{u}_i(x_i,t)$, $I_y = I_z = I$, $E^L I^L = E_i I_i$, and $E^R I^R = E_{i+1} I_{i+1}$. Note that the subscripts i and $i+1$ for the parameters u, E, and I refer to the ith and $(i+1)$th shaft segments, respectively.

Similarly, the substitution of Eqs. (8) and (9) into Eqs. (14*a*) and (14*b*), respectively, yields

$$-EI_z \frac{\partial^2 u_y^R}{\partial x^2} + EI_z \frac{\partial^2 u_y^L}{\partial x^2} + J_{D,i} \frac{\partial^2}{\partial t^2}\left(\frac{\partial u_y}{\partial x}\right) + J_{P,i}\Omega \frac{\partial}{\partial t}\left(\frac{\partial u_z}{\partial x}\right) = 0 \tag{18a}$$

$$-EI_y \frac{\partial^2 u_z^R}{\partial x^2} + EI_y \frac{\partial^2 u_z^L}{\partial x^2} + J_{D,i} \frac{\partial^2}{\partial t^2}\left(\frac{\partial u_z}{\partial x}\right) - J_{P,i}\Omega \frac{\partial}{\partial t}\left(\frac{\partial u_y}{\partial x}\right) = 0 \tag{18b}$$

Since, for the disk i with small thickness h, one has

$$J_{P,i} = 2J_{D,i} \tag{19}$$

introducing Eq. (2) into Eqs. (18*a*) and (18*b*), one obtains

$$-EI \frac{\partial^2 u^R}{\partial x^2} + EI \frac{\partial^2 u^L}{\partial x^2} + J_{D,i}\left(\frac{\partial^3 u(x_i,t)}{\partial x \partial t^2} - j2\Omega \frac{\partial^2 u(x_i,t)}{\partial x \partial t}\right) = 0 \tag{20}$$

or

$$E_i I_i u_i''(x_i,t) = E_{i+1} I_{i+1} u_{i+1}''(x_i,t) - J_{D,i}[\ddot{u}_i'(x_i,t) - j2\Omega \dot{u}_i'(x_i,t)] \tag{21}$$

which is the equilibrium equation for the bending moments on disk i (located at node i).

For a circular thin disk with mass density ρ_d, diameter d_d, and thickness h, its mass m_d and diametrical mass moment of inertia J_D are given by

$$m_d = \rho_d h(\pi d_d^2/4) \tag{22a}$$

$$J_D = \rho_d h(\pi d_d^4/64) \tag{22b}$$

2.3 Conditions for Continuity and Equilibrium at Intermediate Node *i*. The continuity of displacements and slopes for the two shaft segments (i) and $(i+1)$ joined at node i (see Fig. 1) requires that

$$U_i(x_i) = U_{i+1}(x_i) \tag{23a}$$

$$U_i'(x_i) = U_{i+1}'(x_i) \tag{23b}$$

Since the equations for the equilibrium of the shearing forces and bending moments of the two shaft segments (i) and $(i+1)$ joined at disk i are given by Eqs. (17) and (21), the substitution of Eq. (4) into the latter equations produces

$$E_iI_iU_i'''(x_i) = E_{i+1}I_{i+1}U_{i+1}'''(x_i) - m_{d,i}\tilde{\omega}^2U_i(x_i) \tag{24a}$$

$$E_iI_iU_i''(x_i) = E_{i+1}I_{i+1}U_{i+1}''(x_i) + J_{eq,i}\tilde{\omega}^2U'(x_i) \tag{24b}$$

where

$$J_{\text{eq},i} = J_{D,i}[1 \mp 2(\Omega/\tilde{\omega})] = J_{D,i}(1 \mp 2\lambda) \tag{25a}$$

$$\lambda = \Omega/\tilde{\omega} \tag{25b}$$

In Eq. (24*b*), the term $J_{eq,i}\tilde{\omega}^2U'(x_i)$ denotes the gyroscopic moment of disk i, thus, $J_{eq,i}$ represents the (frequency-dependent) equivalent mass moment of inertia of the ith disk. Furthermore, in Eq. (25*a*), the symbol λ denotes the speed ratio, while the upper sign $(-)$ and lower sign $(+)$ are for the "forward" and "backward" whirls, respectively. Substituting $U_i(x)$, which is defined by Eq. (7), into Eqs. (23) and (24), one obtains

$$\begin{aligned} &A_i\sinh\beta_ix_i + B_i\cosh\beta_ix_i + C_i\sin\beta_ix_i + D_i\cos\beta_ix_i \\ &\quad - (A_{i+1}\sinh\beta_{i+1}x_i + B_{i+1}\cosh\beta_{i+1}x_i + C_{i+1}\sin\beta_{i+1}x_i \\ &\quad + D_{i+1}\cos\beta_{i+1}x_i) = 0 \end{aligned} \tag{26a}$$

$$\begin{aligned} &\beta_i(A_i\cosh\beta_ix_i + B_i\sinh\beta_ix_i + C_i\cos\beta_ix_i - D_i\sin\beta_ix_i) \\ &\quad - \beta_{i+1}(A_{i+1}\cosh\beta_{i+1}x_i + B_{i+1}\sinh\beta_{i+1}x_i \\ &\quad + C_{i+1}\cos\beta_{i+1}x_i - D_{i+1}\sin\beta_{i+1}x_i) = 0 \end{aligned} \tag{26b}$$

$$\begin{aligned} &A_i(\cosh\beta_ix_i + Q_i\sinh\beta_ix_i) + B_i(\sinh\beta_ix_i + Q_i\cosh\beta_ix_i) \\ &\quad - C_i(\cos\beta_ix_i - Q_i\sin\beta_ix_i) + D_i(\sin\beta_ix_i + Q_i\cos\beta_ix_i) \\ &\quad - P_{i+1}(A_{i+1}\cosh\beta_{i+1}x_i + B_{i+1}\sinh\beta_{i+1}x_i \\ &\quad - C_{i+1}\cos\beta_{i+1}x_i + D_{i+1}\sin\beta_{i+1}x_i) = 0 \end{aligned} \tag{27a}$$

$$\begin{aligned} &A_i(\sinh\beta_ix_i - S_i\cosh\beta_ix_i) + B_i(\cosh\beta_ix_i - S_i\sinh\beta_ix_i) \\ &\quad - C_i(\sin\beta_ix_i + S_i\cos\beta_ix_i) - D_i(\cos\beta_ix_i - S_i\sin\beta_ix_i) \\ &\quad - R_{i+1}(A_{i+1}\sinh\beta_{i+1}x_i + B_{i+1}\cosh\beta_{i+1}x_i \\ &\quad - C_{i+1}\sin\beta_{i+1}x_i - D_{i+1}\cos\beta_{i+1}x_i) = 0 \end{aligned} \tag{27b}$$

where

$$P_{i+1} = E_{i+1}I_{i+1}\beta_{i+1}^3/(E_iI_i\beta_i^3) \tag{28a}$$

$$Q_i = m_{d,i}\tilde{\omega}^2/(E_iI_i\beta_i^3) \tag{28b}$$

$$R_{i+1} = E_{i+1}I_{i+1}\beta_{i+1}^2/(E_iI_i\beta_i^2) \tag{29a}$$

$$S_i = J_{\text{eq},i}\tilde{\omega}^2\beta_i/(E_iI_i\beta_i^2) \tag{29b}$$

2.4 Boundary Conditions at Two Ends of the Entire Shaft. The presented method is available for various boundary conditions (BCs), but only the shaft-disk system with rigid ball-bearing supports (such as that shown in Fig. 1) is introduced here because of a limitation of space. For Fig. 1, the transverse displacements and bending moments at nodes 0 and n are equal to zero; thus

$$U_1(0) = 0 \tag{30a}$$

$$U_1''(0) = 0 \tag{30b}$$

$$U_n(L) = 0 \tag{31a}$$

$$U_n''(L) = 0 \tag{31b}$$

Introducing Eq. (7) into the preceding equations, one has

$$B_1 + D_1 = 0 \tag{32a}$$

$$B_1 - D_1 = 0 \tag{32b}$$

$$A_n\sinh\beta_nL + B_n\cosh\beta_nL + C_n\sin\beta_nL + D_n\cos\beta_nL = 0 \tag{33a}$$

$$A_n\sinh\beta_nL + B_n\cosh\beta_nL - C_n\sin\beta_nL - D_n\cos\beta_nL = 0 \tag{33b}$$

Since the supporting condition of the present rotating shaft is similar to that of the pinned-pinned (P-P) *stationary* beam, it is called the P-P shaft in this paper, for convenience.

2.5 Determination of Whirling Speeds and Mode Shapes. For the shaft-disk system consisting of n shaft segments and carrying $n-1$ rigid disks as shown in Fig. 1, from the last section one sees that there exist simultaneous equations for the integration constants of all shaft segments to take the form

$$[H(\tilde{\omega})]_{\bar{n}\times\bar{n}}\{B\}_{\bar{n}\times1} = 0 \quad (\text{with } \bar{n} = 4n) \tag{34}$$

where $\{B\}_{\bar{n}\times1}$ is a column vector composed of the $\bar{n}$ integration constants for all of the n shaft segments, i.e.,

$$\{B\} = [A_1 \quad B_1 \quad C_1 \quad D_1 \ldots A_i \quad B_i \quad C_i \quad D_i \ldots A_n \quad B_n \quad C_n \quad D_n]^T \tag{35}$$

and $[H]_{\bar{n}\times\bar{n}}$ is an $\bar{n}\times\bar{n}$ square matrix. For the P-P shafting system shown in Fig. 1, the nonzero coefficients of $[H]_{\bar{n}\times\bar{n}}$ may be obtained from Eqs. (32), (26), (27), and (33), respectively.

2.5.1 For the Left Pinned End at Node 0. From Eqs. (32) one obtains

$$H_{1,1} = 0 \tag{36a}$$

$$H_{1,2} = 1 \tag{36b}$$

$$H_{1,3} = 0 \tag{36c}$$

$$H_{1,4} = 1 \tag{36d}$$

$$H_{2,1} = 0 \tag{37a}$$

$$H_{2,2} = 1 \tag{37b}$$

$$H_{2,3} = 0 \tag{37c}$$

$$H_{2,4} = -1 \tag{37d}$$

2.5.2 For the Intermediate Node i (With Total Number of Shaft Segments $n \geq 2$). From Eqs. (26) and (27) one obtains

$$H_{4i-1,4i-3} = \sinh\beta_ix_i \tag{38a}$$

$$H_{4i-1,4i-2} = \cosh\beta_ix_i \tag{38b}$$

$$H_{4i-1,4i-1} = \sin\beta_ix_i \tag{38c}$$

$$H_{4i-1,4i} = \cos\beta_ix_i \tag{38d}$$

$$H_{4i-1,4i+1} = -\sinh\beta_{i+1}x_i \tag{38e}$$

$$H_{4i-1,4i+2} = -\cosh\beta_{i+1}x_i \tag{38f}$$

$$H_{4i-1,4i+3} = -\sin\beta_{i+1}x_i \tag{38g}$$

$$H_{4i-1,4i+4} = -\cos\beta_{i+1}x_i \tag{38h}$$

$$H_{4i,4i-3} = \beta_i\cosh\beta_ix_i \tag{39a}$$

$$H_{4i,4i-2} = \beta_i\sinh\beta_ix_i \tag{39b}$$

$$H_{4i,4i-1} = \beta_i\cos\beta_ix_i \tag{39c}$$

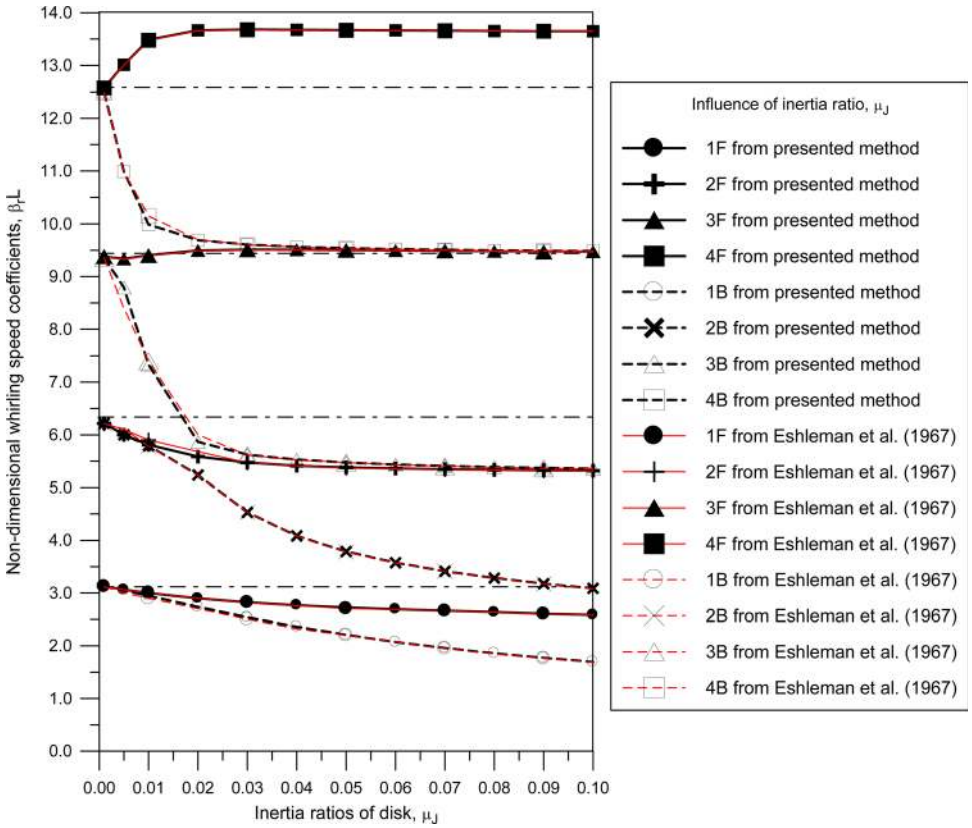

Fig. 5 Influence of the inertia ratio μ_J on the lowest four nondimensional whirling speed coefficients $\beta_r L$ ($r = 1 - 4$), for the P-P shaft carrying a single disk at $x = x_1 = 0.25\,L$ (cf., Fig. 6(*a*)) with the speed ratio $\lambda = \Omega/\tilde{\omega}_r = 1.0$

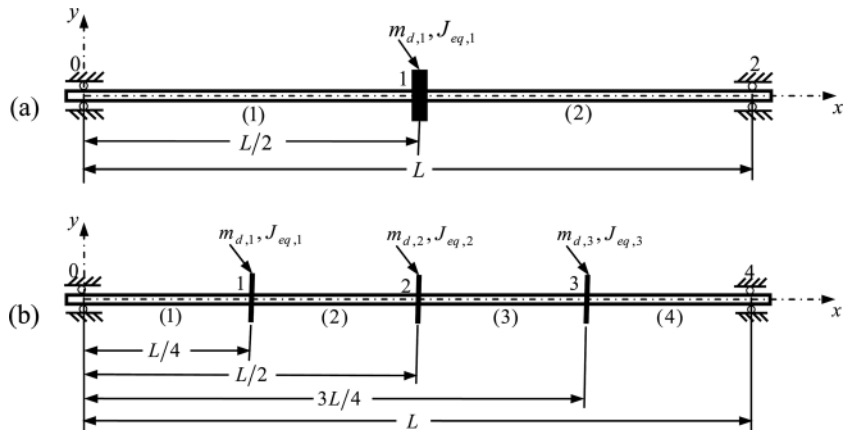

Fig. 6 A uniform P-P shaft carrying (*a*) one single disk (with thickness $h = 0.012$ m) at its center ($x_1 = L/2$), and (*b*) three identical rigid disks (with $h_1 = h_1 = h_1 = h/3 = 0.004$ m) at $x_1 = L/4$, $x_2 = L/2$ and $x_3 = 3\,L/4$, respectively

$$H_{4i,4i} = -\beta_i \sin \beta_i x_i \tag{39d}$$

$$H_{4i,4i+1} = -\beta_{i+1} \cosh \beta_{i+1} x_i \tag{39e}$$

$$H_{4i,4i+2} = -\beta_{i+1} \sinh \beta_{i+1} x_i \tag{39f}$$

$$H_{4i,4i+3} = -\beta_{i+1} \cos \beta_{i+1} x_i \tag{39g}$$

$$H_{4i,4i+4} = \beta_{i+1} \sin \beta_{i+1} x_i \tag{39h}$$

$$H_{4i+1,4i-3} = \cosh\beta_i x_i + Q_i \sinh\beta_i x_i \tag{40a}$$

$$H_{4i+1,4i-2} = \sinh\beta_i x_i + Q_i \cosh\beta_i x_i \tag{40b}$$

$$H_{4i+1,4i-1} = -(\cos\beta_i x_i - Q_i \sin\beta_i x_i) \tag{40c}$$

$$H_{4i+1,4i} = \sin\beta_i x_i + Q_i \cos\beta_i x_i \tag{40d}$$

$$H_{4i+1,4i+1} = -P_{i+1} \cosh\beta_{i+1} x_i \tag{40e}$$

$$H_{4i+1,4i+2} = -P_{i+1} \sinh\beta_{i+1} x_i \tag{40f}$$

$$H_{4i+1,4i+3} = P_{i+1} \cos\beta_{i+1} x_i \tag{40g}$$

Table 1 The lowest five natural frequencies $\omega_1 - \omega_5$ (with $\lambda = 0$) and whirling speeds $\tilde{\omega}_1 - \tilde{\omega}_5$ (with $\lambda = 1.0$) for the P-P shaft carrying a single central rigid disk (see Fig. 6(*a*)) obtained from the presented method and the FEM (with 60 shaft elements and 240 effective dofs)

		Natural frequencies ω_r (rad/s) with $\lambda = 0$					
Methods	Direction of whirling	ω_1	ω_2	ω_3	ω_4	ω_5	CPU time (s)
Presented	—	63.9603	401.5251	1139.5836	1232.5813	3601.9354	1
FEM	—	63.9603	401.5251	1139.5838	1232.5815	3601.9431	5
—	—	Whirling speeds $\tilde{\omega}_r$ (rad/s) with $\lambda = 1.0$					
—	—	$\tilde{\omega}_1^F$ or $\tilde{\omega}_1^B$	$\tilde{\omega}_2^F$ or $\tilde{\omega}_2^B$	$\tilde{\omega}_3^F$ or $\tilde{\omega}_3^B$	$\tilde{\omega}_4^F$ or $\tilde{\omega}_4^B$	$\tilde{\omega}_5^F$ or $\tilde{\omega}_5^B$	CPU time (s)
Presented	Forward	63.9603	986.0439	1139.5836	3523.6775	3603.8514	2
	Backward	63.9603	252.7240	1139.5836	1142.4114	3574.9815	
FEM	Forward	63.9603	986.0441	1139.5838	3523.6850	3603.8591	10
	Backward	63.9603	252.7240	1139.5838	1142.4116	3574.9892	

$$H_{4i+1,4i+4} = -P_{i+1}\sin\beta_{i+1}x_i \tag{40h}$$

$$H_{4i+2,4i-3} = \sin h\beta_i x_i - S_i\cos h\beta_i x_i \tag{41a}$$

$$H_{4i+2,4i-2} = \cos h\beta_i x_i - S_i\sin h\beta_i x_i \tag{41b}$$

$$H_{4i+2,4i-1} = -(\sin\beta_i x_i + S_i\cos\beta_i x_i) \tag{41c}$$

$$H_{4i+2,4i} = -(\cos\beta_i x_i - S_i\sin\beta_i x_i) \tag{41d}$$

$$H_{4i+2,4i+1} = -R_{i+1}\sin h\beta_{i+1}x_i \tag{41e}$$

$$H_{4i+2,4i+2} = -R_{i+1}\cos h\beta_{i+1}x_i \tag{41f}$$

$$H_{4i+2,4i+3} = R_{i+1}\sin\beta_{i+1}x_i \tag{41g}$$

$$H_{4i+2,4i+4} = R_{i+1}\cos\beta_{i+1}x_i \tag{41h}$$

2.5.3 For the Right Pinned End at Node n. From Eqs. (33) one obtains

$$H_{4n-1,4n-3} = \sinh\beta_n L \tag{42a}$$

$$H_{4n-1,4n-2} = \cosh\beta_n L \tag{42b}$$

$$H_{4n-1,4n-1} = \sin\beta_n L \tag{42c}$$

$$H_{4n-1,4n} = \cos\beta_n L \tag{42d}$$

$$H_{4n,4n-3} = \sinh\beta_n L \tag{43a}$$

$$H_{4n,4n-2} = \cosh\beta_n L \tag{43b}$$

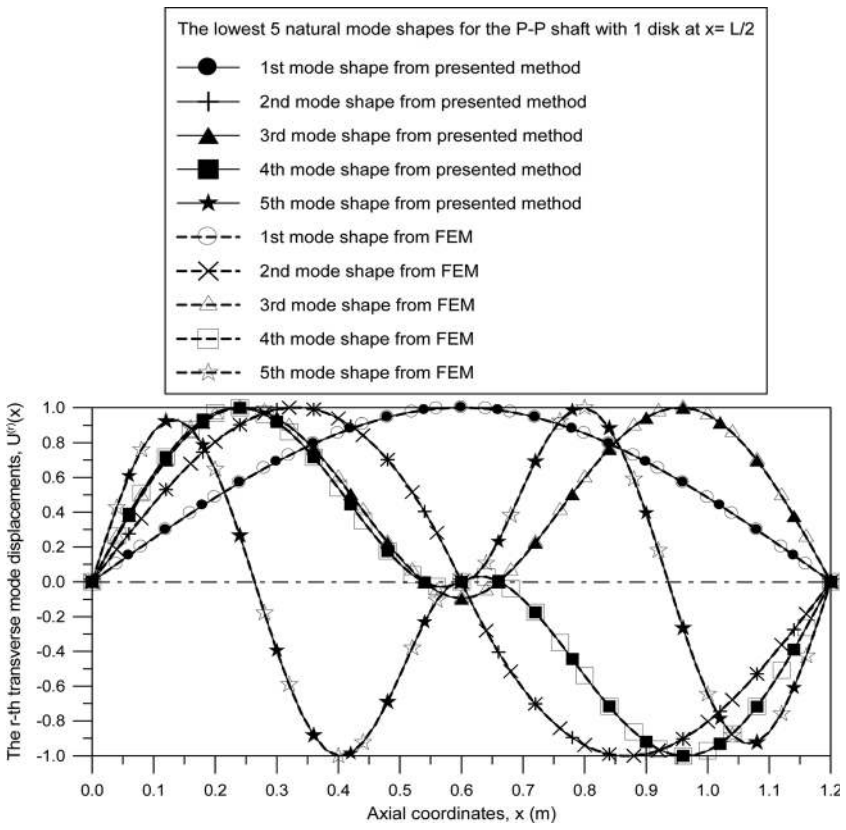

Fig. 7 The lowest five natural mode shapes for the P-P shaft carrying a single central rigid disk (see Fig. 6(*a*)) (with the speed ratio $\lambda = 0$) obtained from the presented method (denoted by solid lines: —) and the FEM (denoted by dashed lines: - - -)

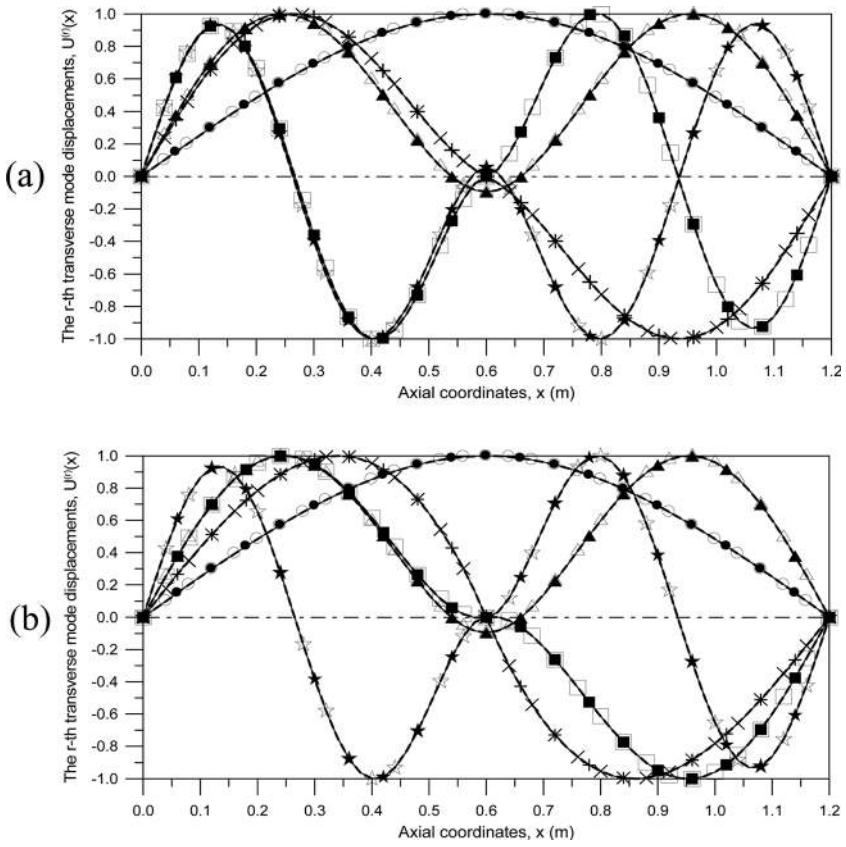

Fig. 8 The lowest five (whirling) mode shapes of the P-P shaft carrying a single rigid disk (see Fig. 6(*a*)) obtained from the presented method (denoted by the solid lines: —) and the FEM (denoted by the dashed lines: - - -) with the speed ratio $\lambda = 1.0$ for (*a*) forward whirling, and (*b*) backward whirling

$$H_{4n,4n-1} = -\sin\beta_n L \tag{43c}$$

$$H_{4n,4n} = -\cos\beta_n L \tag{43d}$$

The nontrivial solution for Eq. (34) requires that

$$|H(\tilde{\omega})| = 0 \tag{44}$$

The preceding expression is an eigenvalue equation, from which one may determine the whirling speeds of the shaft-disk system $\tilde{\omega}_r$ ($r = 1, 2, 3, \ldots$) by using the half-interval method [17,18] and, corresponding to each whirling speed $\tilde{\omega}_r$, one may obtain the associated integration constants A_i, B_i, C_i, and D_i ($i = 1$ to n), from Eq. (34). The substitution of the latter constants into Eq. (7) will define the corresponding rth whirling mode shape of the entire shaft, $U^{(r)}(x) = \sum_{i=1}^{n} U_i^{(r)}(x)$.

3 Numerical Results and Discussions

3.1 Comparisons With Existing Literature. For a uniform P-P shaft carrying a rigid disk at $x = L/4$ (cf. Figure 6(*a*)), the relationships between the inertia ratio $\mu_J = (d_d/4L)^2$ and the lowest four nondimensional whirling speed coefficients $\beta_r L = \sqrt[4]{\rho_s A_s L^4 \tilde{\omega}_r^2/(EI)}$ ($r = 1 - 4$) are shown in Fig. 5, in which the thick solid lines (—) and dashed lines (- - -) are for the forward and backward whirls obtained from the presented method, respectively, while the thin solid lines (—) and dashed lines (- - -) are for the forward and backward whirls obtained from Fig. 5 of Eshleman and Eubanks [4], respectively. Furthermore, the symbols, ● (or ○), + (or ×), ▲ (or △), and ■ (or □) denote the 1st, 2nd, 3rd, and 4th whirling speed coefficients, respectively. From Fig. 5, one sees that the results of the presented method are in good agreement with those of Eshleman and Eubanks [4]. The given data for Fig. 5 are as follows: $L = 1.26$ m, shaft diameter $d_s = 0.1\,L = 0.126$ m, disk thickness $h = L/72 = 0.0175$ m and disk diameter $d_d = 4L\sqrt{\mu_J} = 5.04\sqrt{\mu_J}$, speed ratio $\lambda = \Omega/\tilde{\omega}_r = 1.0$, Young's modulus $E = 2.068 \times 10^{11}$ N/m^2, and mass density $\rho_s = \rho_d = 7850$ kg/m^3, where the inertia ratio (μ_J) is given by

$$\mu_J = J_D/(m_d L^2) = [\rho_d(\pi d_d^4/64)h]/[\rho_d(\pi d_d^2/4)hL^2] = [d_d/(4L)]^2 \tag{45}$$

3.2 Free Vibrations and Whirling Motions of a P-P Shaft Carrying Multiple Disks. Figure 6 shows the uniform P-P shaft mounted by one disk and three disks, respectively, studied here. If h represents the thickness of the disk for the case of the shaft carrying one single disk (see Fig. 6(*a*)), then for the case of the shaft carrying three identical disks (see Fig. 6(*b*)), the thickness of each disk is assumed to be $h_i = h/3$ with $i = 1 - 3$. The dimensions and material constants of the shaft-disk system are as follows: shaft diameter $d_s = 0.02$ m, shaft length $L = 1.20$ m, disk diameter $d_d = 0.36$ m, thickness of a single disk $h = 0.012$ m, Young's modulus $E = 2.068 \times 10^{11}$ N/m^2, and the mass density for the shaft (or disk) material is $\rho_s = \rho_d = 7850$ kg/m^3.

For the P-P shaft carrying a single rigid disk at its center (with $x = x_1 = L/2$), as shown in Fig. 6(*a*), the characteristic equations are similar to Eqs. (34)–(44). If the rth natural frequency for the transverse vibrations of the stationary P-P shaft-disk system is denoted by ω_r (with $r = 1, 2, \ldots$), then the lowest five natural frequencies obtained from the presented method and the FEM (with 60 shaft elements and 240 effective dofs) are listed in the 3rd and 4th rows of Table 1, respectively. Since $\Omega = 0$ for a stationary shaft, the foregoing natural frequencies $\omega_1 - \omega_5$ (rad/s) are

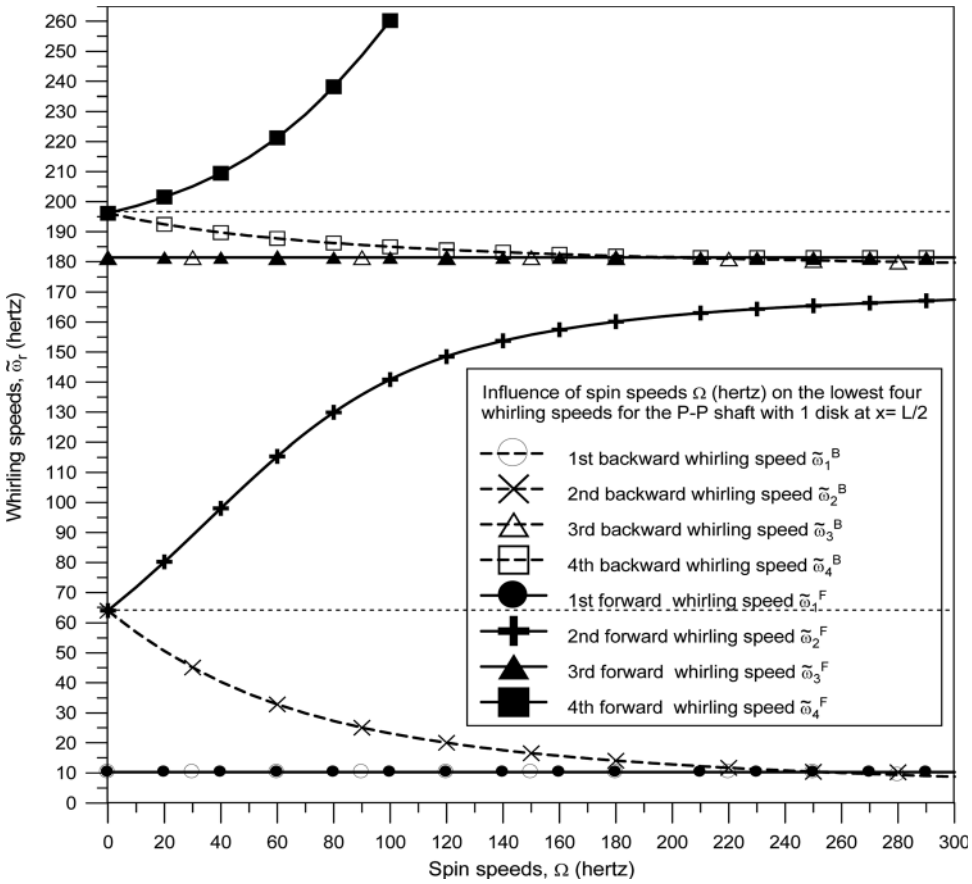

Fig. 9 Influence of the spin speeds Ω on the lowest four whirling speeds ($\tilde{\omega}_1$–$\tilde{\omega}_4$) for the P-P shaft carrying 1 central rigid disk (see Fig. 6(*a*)) obtained from the presented method

determined with zero speed ratio ($\lambda = \Omega/\tilde{\omega} = 0$) and, in such a case, one has $\tilde{\omega}_r = \omega_r$. From Table 1, one sees that the values of $\omega_1 - \omega_5$ (rad/s) obtained from the presented method and those obtained from the FEM are in good agreement, but the CPU time required by the presented method is about one fifth of that required by the FEM (by using an IBM PC Pentium III).

For the case of $\lambda = 1.0$, the lowest five forward whirling speeds $\tilde{\omega}_r^F$ and backward ones $\tilde{\omega}_r^B$ with $r = 1 - 5$, obtained from the presented method are listed in the 7th and 8th rows of Table 1, while the corresponding ones obtained from the FEM are listed in the final two rows of the table. It is seen that the results of the two methods are also in good agreement. From Table 1 one also sees that, either obtained from the presented method or the FEM, there exist the relationships $\tilde{\omega}_1^F = \tilde{\omega}_1^B = \omega_1$ and $\tilde{\omega}_3^F = \tilde{\omega}_3^B = \omega_3$; this is because the slopes of the 1st and 3rd natural mode shapes at $x = x_1 = L/2$ (where the rigid disk is located) are equal to zero (see Fig. 7), so that the gyroscopic moments induced by the rigid disk associated with the 1st and 3rd modes are equal to zero.

Corresponding to the lowest five natural frequencies listed in the 3rd and 4th rows of Table 1, the lowest five natural mode shapes of the P-P shaft-disk system are plotted in Fig. 7, in which, the mode shapes obtained from the presented method are denoted by the solid lines (—) and those from the FEM by the dashed lines (- - -). Furthermore, the 1st, 2nd, 3rd, 4th, and 5th natural mode shapes are denoted by the symbols ● (or ○), + (or ×), ▲ (or △), ■ (or □) and ★ (or ☆), respectively. From Fig. 7, one sees that the mode shapes obtained from the presented method and those obtained from the FEM are overlapped, because the corresponding natural frequencies listed in Table 1 are very close to each other.

Corresponding to the lowest five whirling speeds ($\tilde{\omega}_1 - \tilde{\omega}_5$) listed in the final four rows of Table 1, the lowest five mode shapes of the shaft-disk system for forward and backward whirls are plotted in Figs. 8(*a*) and 8(*b*), respectively. It is noted that the 1st and 3rd forward whirling mode shapes in Fig. 8(*a*) are the same as the 1st and 3rd backward ones in Fig. 8(*b*) and they are also identical to the 1st and 3rd natural mode shapes in Fig. 7, respectively; this is because $\tilde{\omega}_1^F = \tilde{\omega}_1^B = \omega_1$ and $\tilde{\omega}_3^F = \tilde{\omega}_3^B = \omega_3$ as previously mentioned. Comparing Fig. 8(*a*) with Fig. 8(*b*), one sees that, except for the 1st and 3rd mode shapes, the 2nd, 4th, and 5th forward whirling mode shapes are different from the corresponding backward ones, because the corresponding 2nd, 4th, and 5th forward whirling speeds ($\tilde{\omega}_2^F$, $\tilde{\omega}_4^F$, and $\tilde{\omega}_5^F$) are different from the corresponding backward ones ($\tilde{\omega}_2^B$, $\tilde{\omega}_4^B$, and $\tilde{\omega}_5^B$), as one may see from Table 1. Figures 8(*a*) and 8(*b*) also reveal that all whirling mode shapes obtained from the presented method are in good agreement with those obtained from the FEM (using the technique shown in the Appendix). Therefore, only the curves of the whirling speeds $\tilde{\omega}_r$ versus the spin speeds Ω obtained from the presented method are plotted in Fig. 9.

In Fig. 9, the relationships between $\tilde{\omega}_1^F - \tilde{\omega}_4^F$ (Hz) and Ω (Hz) are denoted by the solid lines (—), while those between $\tilde{\omega}_1^B - \tilde{\omega}_4^B$ and Ω are denoted by the dashed lines (- - -), with the symbols, ● (or ○), + (or ×), ▲ (or △) and ■ (or □) denoting the 1st, 2nd, 3rd, and 4th modes, respectively. From the figure one sees that $\tilde{\omega}_1^F = \tilde{\omega}_1^B = \omega_1 = 63.9603$ rad/s ≈ 10.18 Hz and $\tilde{\omega}_3^F = \tilde{\omega}_3^B = \omega_3 = 1139.5836$ rad/s ≈ 181.37 Hz; in other words, the spin speed Ω does not affect the 1st and 3rd whirling speeds because the slopes of the 1st and 3rd natural mode shapes at the position $x = x_1 = L/2$ (where the single disk located) are equal to zero. Zu and Han [5] have shown that, for a beam being put into a spinning motion, its at-rest (transverse-vibration) natural frequency will split into two components: forward and backward precessions. This is the reason why, in Fig. 9, each pair of (forward) solid lines and (backward) dashed lines meet at a point on the vertical

Table 2 The lowest five natural frequencies $\omega_1 - \omega_5$ (with $\lambda = 0$) and whirling speeds $\tilde{\omega}_1 - \tilde{\omega}_5 1$ (with $\lambda = 1.0$) for the P-P shaft carrying three identical rigid disks (see Fig. 6(*b*)) obtained from presented method and FEM (with 60 shaft elements and 240 effective dofs)

		Natural frequencies ω_r (rad/s) with $\lambda = 0$					
Methods	Direction of whirling	ω_1	ω_2	ω_3	ω_4	ω_5	CPU time (s)
Presented	—	75.3973	290.8641	611.9586	958.4773	1288.8920	1
FEM	—	75.3973	290.8641	611.9586	958.4773	1288.8920	5
—	—	Whirling speeds $\tilde{\omega}_r$ (rad/s) with $\lambda = 1.0$					
—	—	$\tilde{\omega}_1^F$ or $\tilde{\omega}_1^B$	$\tilde{\omega}_2^F$ or $\tilde{\omega}_2^B$	$\tilde{\omega}_3^F$ or $\tilde{\omega}_3^B$	$\tilde{\omega}_4^F$ or $\tilde{\omega}_4^B$	$\tilde{\omega}_5^F$ or $\tilde{\omega}_5^B$	CPU time (s)
Presented	Forward	77.1099	316.2592	686.8000	4406.5020	4412.7430	2
	Backward	73.7624	266.5857	513.7804	587.4075	927.6585	
FEM	Forward	77.1099	316.2592	686.8000	4406.5176	4412.7581	10
	Backward	73.7624	266.5857	513.7804	587.4075	927.6585	

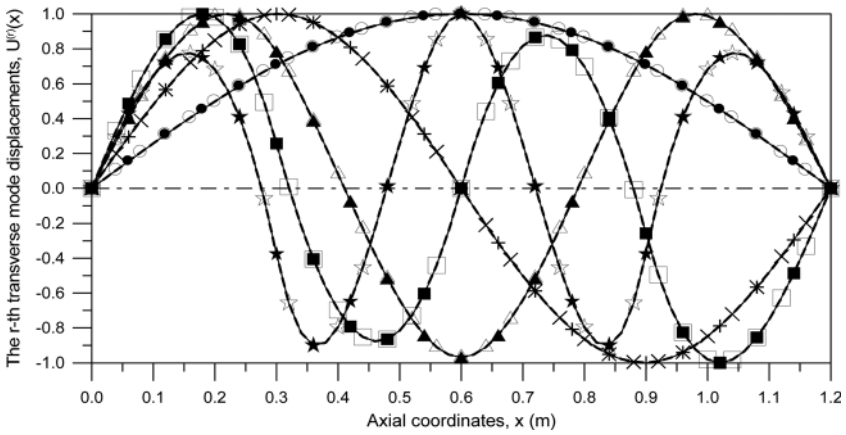

Fig. 10 The lowest five natural mode shapes for the P-P shaft carrying three identical rigid disks (see Fig. 6(*b*)) (with the speed ratio $\lambda = 0$). The legends are the same as those of Fig. 7.

(ordinate) axis with $\Omega = 0$ and $\tilde{\omega}_r^F = \tilde{\omega}_r^B = \omega_r$. In addition, Fig. 9 also indicates that the influence of the spin speed Ω on the 2nd whirling speed, either $\tilde{\omega}_2^F$ or $\tilde{\omega}_2^B$, is much greater than that on the 4th whirling speed; this is because the slope of the 2nd natural mode shape at the position $x = L/2$ is much greater than the corresponding slope of the 4th one, as one may see from Fig. 7. From the foregoing analyses one sees that the influence of the spin speed Ω on the rth whirling speed $\tilde{\omega}_r$ is dependent on the slope of the corresponding rth natural mode shape at the position where the rigid disk is located.

For the uniform P-P shaft carrying three identical rigid disks (with thickness $h_1 = h_2 = h_3 = h/3 = 0.004$ m) at $x_1 = L/4$, $x_2 = L/2$, and $x_3 = 3L/4$, respectively) as shown in Fig. 6(*b*), the lowest five natural frequencies ω_r are listed in the 3rd and 4th rows of Table 2 (with $\lambda = 0$), while the lowest five forward whirling speeds $\tilde{\omega}_r^F$ ($r = 1 - 5$) and backward ones $\tilde{\omega}_r^B$ ($r = 1 - 5$) obtained from the presented method and the FEM are listed in the final four rows of Table 2 (with $\lambda = 1.0$). Although the configuration of the shaft-disk system shown in Fig. 6(*b*) is symmetrical and so are the 1st, 3rd, and 5th natural mode shapes shown in Fig. 10, one cannot find the slopes of any natural mode shape at the three positions $x_1 = L/4$, $x_2 = L/2$, and $x_3 = 3L/4$ (where the three disks are located) to be equal to zero simultaneously. This is the reason why one cannot find the relationship $\tilde{\omega}_r^F = \tilde{\omega}_r^B = \omega_r$ from Table 2. Therefore, the lowest five forward whirling mode shapes are different from the backward ones and thus are between the curves of $\tilde{\omega}_r^F$ versus Ω and the corresponding ones of $\tilde{\omega}_r^B$ versus Ω, as one may see from the computer output (not shown here). In other words, for a shaft carrying more than one rigid disk, the possibility of $\tilde{\omega}_r^F = \tilde{\omega}_r^B = \omega_r$ (with $\lambda \neq 0$) is small, because it is difficult to find the slopes of any natural mode shape at the positions where the rigid disks are located to be equal to zero simultaneously.

4 Conclusions

(1) With the transverse displacement of each shaft cross-section represented by a complex number and the effects of each rigid disk i replaced by a lumped mass $m_{d,i}$ together with a frequency-dependent equivalent mass moment of inertia $J_{eq,i}$, one may easily obtain the forward and backward whirling speeds ($\tilde{\omega}_r^F$ and $\tilde{\omega}_r^B$) and the associated whirling mode shapes for a rotating shaft mounted by arbitrary rigid disks by using the simple approach presented in this paper.

(2) When a shaft-disk system is put into a spinning motion, each of its at-rest (transverse-vibration) natural frequencies ω_r ($r = 1, 2, ...$) will split into two branches: forward speeds $\tilde{\omega}_r^F$ and backward speeds $\tilde{\omega}_r^B$, where the right superscripts "F" and "B" denote *f*orward and backward whirls, respectively.

(3) The influence of the spin speed Ω on the rth whirling speed and mode shape is dependent on the slopes of the corresponding rth natural mode shape at the positions where the rigid disks are located: The larger the slopes, the larger the influence of the spin speed on the whirling speed and mode shape, because the magnitude of the gyroscopic moment

induced by a rigid disk is proportional to the magnitude of the slope of the natural mode shape at the position where the rigid disk is located.

(4) For a uniform P-P shaft carrying one central rigid disk, the slopes of the 1st and 3rd natural mode shapes at $x = 0.5L$ (where the rigid disk is located) are equal to zero; for this reason, there exist the relationships $\tilde{\omega}_1^F = \tilde{\omega}_1^B = \omega_1$ and $\tilde{\omega}_3^F = \tilde{\omega}_3^B = \omega_3$ and the influence of the spin speed Ω on the 1st and 3rd whirling speeds and mode shapes is nil. However, for the same shaft carrying more than one rigid disk, the possibility of $\tilde{\omega}_r^F = \tilde{\omega}_r^B = \omega_r$ (with $\lambda \neq 0$) is small, because it is difficult to find the slopes of any natural mode shape at the positions where a number of rigid disks are located to be equal to zero simultaneously.

(5) Since the order of the characteristic equation obtained from the presented method is much lower than that obtained from the FEM, the CPU time required by the former is much less than that required by the latter. This is another predominant advantage for the presented method to be superior to the FEM, in addition to providing the "exact" solutions for evaluating the accuracy of the other "approximate" ones. Furthermore, the formulation of the proposed method is also much simpler than that of the FEM, as one may see from the existing literature and the Appendix of this paper.

Acknowledgment

This paper is part of the project with Contract No. NSC99-2221-E-006-241. The financial support of the National Science Council, Republic of China, is highly appreciated.

Appendix: Determination of Whirling Speeds and Mode Shapes by the FEM

According to Nelson and McVaugh [9] and Yamamoto and Ishida [11], the equations of motion for the free vibration of a "rotating" shaft-disk system take the form

$$[\bar{m}]\{\ddot{\bar{u}}\} + [\bar{c}]\{\dot{\bar{u}}\} + [\bar{k}]\{\bar{u}\} = 0 \tag{A1}$$

where $[\bar{m}]$, $[\bar{c}]$, and $[\bar{k}]$ are the effective overall mass, damping, and stiffness matrices of the entire shaft-disk system, respectively, and $\{\bar{u}\}$, $\{\dot{\bar{u}}\}$, and $\{\ddot{\bar{u}}\}$ are the associated displacement, velocity, and acceleration vectors, respectively. In order to solve Eq. (A1) by using the existing computer codes in Ref. [19], one needs to transform it into the following form [16]:

$$[\bar{M}]\{\dot{\bar{U}}\} + [\bar{K}]\{\bar{U}\} = 0 \tag{A2}$$

where

$$[\bar{M}] = \begin{bmatrix} [0] & [\bar{m}] \\ [\bar{m}] & [\bar{c}] \end{bmatrix} \tag{A3a}$$

$$[\bar{K}] = \begin{bmatrix} -[\bar{m}] & [0] \\ [0] & [\bar{k}] \end{bmatrix} \tag{A3b}$$

$$\{\bar{U}\} = \begin{Bmatrix} \{\dot{\bar{u}}\} \\ \{\bar{u}\} \end{Bmatrix} \tag{A3c}$$

$$\{\dot{\bar{U}}\} = \begin{Bmatrix} \{\ddot{\bar{u}}\} \\ \{\dot{\bar{u}}\} \end{Bmatrix} \tag{A3d}$$

The rth eigenvalues $\tilde{\omega}_r$ and associated rth eigenvectors $[\psi_r]$ of Eq. (A2) take the two pairs of conjugate complex numbers

$$\tilde{\omega}_r^B = \tilde{\omega}_{r,R}^B \pm j\tilde{\omega}_{r,I}^B \tag{A4a}$$

$$\{\psi_r^B\} = \begin{Bmatrix} \tilde{\omega}_{r,R}^B \psi_{r,R}^B \\ \psi_{r,R}^B \end{Bmatrix} \pm j \begin{Bmatrix} \tilde{\omega}_{r,I}^B \psi_{r,I}^B \\ \psi_{r,I}^B \end{Bmatrix} \tag{A4b}$$

$$\tilde{\omega}_r^F = \tilde{\omega}_{r,R}^F \pm j\tilde{\omega}_{r,I}^F \tag{A5a}$$

$$\{\psi_r^F\} = \begin{Bmatrix} \tilde{\omega}_{r,R}^F \psi_{r,R}^F \\ \psi_{r,R}^F \end{Bmatrix} \pm j \begin{Bmatrix} \tilde{\omega}_{r,I}^F \psi_{r,I}^F \\ \psi_{r,I}^F \end{Bmatrix} \tag{A5b}$$

In the preceding equations, the superscripts B and F refer to the "backward" and "forward" whirls, respectively, while the subscripts R and I refer to the "real" and "imaginary" parts of a complex number, respectively, and $j = \sqrt{-1}$. Furthermore, the imaginary parts of $\tilde{\omega}_r$, $\tilde{\omega}_{r,I}^B$, and $\tilde{\omega}_{r,I}^F$ denote the "backward" and "forward" whirling speeds, respectively, while the corresponding real parts of $\{\psi_r\}$, $\{\psi_{r,R}^B\}$, and $\{\psi_{r,R}^F\}$ denote the "backward" and "forward" whirling mode shapes, respectively.

For an undamped "stationary" shaft-disk system, because $\Omega = 0$, Eq. (A1) reduces to

$$[\bar{m}]\{\ddot{\bar{u}}\} + [\bar{k}]\{\bar{u}\} = 0 \tag{A6}$$

which is the equation of motion for the general free vibrations and can be solved with the Jacobi method [20]. The order of the property matrices of Eq. (A2) is two times that of Eq. (A6); this is one of the reasons why the CPU time required by the whirling problem is much greater than that required by the general free vibration problem.

References

[1] Prohl, M. A., 1945, "A General Method for Calculating Critical Speeds of Flexible Rotors," ASME J. Appl. Mech., **12**, pp. 142–148.
[2] Myklestad, N. O., 1944, "A New Method of Calculating Natural Modes of Uncoupled Bending Vibration of Airplane Wings and Other Types of Beams," J. Aeronaut. Sci., **11**, pp. 153–162.
[3] Green, R. B., 1948, "Gyroscopic Effects on the Critical Speeds of Flexible Rotors," ASME J. Appl. Mech., **15**, pp. 369–376.
[4] Eshleman, R. L., and Eubanks, R. A., 1967, "On the Critical Speeds of a Continuous Shaft-Disk System," ASME J. Eng. Ind., **89**, pp. 645–652.
[5] Zu, W. Z., and Han, P. S., 1992, "Natural Frequencies and Normal Modes of Spinning Timoshenko Beam With General Boundary Conditions," ASME J. Appl. Mech., **59**, pp. 197–204.
[6] Shiau, T. N., and Hwang, J. L., 1989, "A New Approach to the Dynamic Characteristic of Undamped Rotor-Bearing Systems," ASME J. Vib., Stress, Reliab. Des., **111**, pp. 379–385.
[7] Firoozian, R., and Zhu, H., 1991, "A Hybrid Method for the Vibration Analysis of Rotor-Bearing Systems," Proc. Inst. Mech. Eng., Part C: J. Mech. Eng. Sci., **25**, pp. 131–137.
[8] Aleyaasin, M., Ebrahimi, M., and Whalley, R., 2000, "Multivariable Hybrid Models for Rotor-Bearing Systems," J. Sound Vib., **233**, pp. 835–856.
[9] Nelson, H. D., and McVaugh, J. M., 1976, "The Dynamics of Rotor-Bearing Systems Using Finite Elements," ASME J. Eng. Ind., **98**, pp. 593–600.
[10] Nelson, H. D., 1980, "A Finite Rotating Shaft Element Using Timoshenko Beam Theory," ASME J. Mech. Des., **102**, pp. 793–803.
[11] Yamamoto, T., and Ishida, Y., 2001, *Linear and Nonlinear Rotordynamics: A Modern Treatment With Applications* (Wiley Series in Nonlinear Science), John Wiley and Sons, New York.
[12] Liu, W. H., and Huang, C. C., 1988, "Vibrations of a Constrained Beam Carrying a Heavy Tip Body," J. Sound Vib., **123**, pp. 15–29.
[13] Wu, J. S., and Chou, H. M., 1999, "A New Approach for Determining the Natural Frequencies and Mode Shapes of a Uniform Beam Carrying any Number of Sprung Masses," J. Sound Vib., **220**, pp. 451–468.
[14] Lin, H. Y., 2008, "On the Natural Frequencies and Mode Shapes of a Multi-Span and Multi-Step Beam Carrying a Number of Concentrated Elements," Struct. Eng. Mech., **29**(5), pp. 531–550.
[15] Przemieniecki, J. S., 1968, *Theory of Matrix Structural Analysis*, McGraw-Hill, New York.
[16] Meirovitch, L., 1967, *Analytical Methods in Vibrations*, Macmillan, London.
[17] Carnahan, B., Luther, H. A., and Wilkes, J. O., 1969, *Applied Numerical Methods*, John Wiley and Sons, New York.
[18] Wu, J. S., and Chen, Y. C., 2011, "Out-of-Plane Free Vibrations of a Horizontal Circular Curved Beam Carrying Arbitrary Sets of Concentrated Elements," J. Struct. Eng., **137**, pp. 220–241.
[19] Garbow, B. S., 1977, *Matrix Eigensystem Routines—EISPACK Guide Extension*, Springer-Verlag, Berlin.
[20] Bathe, K. J., 1982, *Finite Element Procedures in Engineering Analysis*, Prentice-Hall International, New York.